PROCEEDINGS OF SPIE

SPIEDigitalLibrary.org/conference-proceedings-of-spie

Liquid-crystal polarization volume gratings for near-eye displays

Yin, Kun, Zhan, Tao, Xiong, Jianghao, He, Ziqian, Li, Kun, et al.

Kun Yin, Tao Zhan, Jianghao Xiong, Ziqian He, Kun Li, Shin-Tson Wu, "Liquid-crystal polarization volume gratings for near-eye displays," Proc. SPIE 11708, Advances in Display Technologies XI, 1170804 (5 March 2021); doi: 10.1117/12.2577992

SPIE.

Event: SPIE OPTO, 2021, Online Only

Liquid-crystal polarization volume gratings for near-eye displays

Kun Yin,[1] Tao Zhan,[1] Jianghao Xiong,[1] Ziqian He,[1] Kun Li,[2] and Shin-Tson Wu[1]
[1]College of Optics and Photonics, University of Central Florida, Orlando, FL 32816, USA
[2]Goertek Electronics, 5451 Great America Parkway, Suite 301, Santa Clara, CA 95054, USA

ABSTRACT

Liquid crystal-based reflective polarization volume gratings (PVGs), also known as a linear Bragg–Berry phase optical element or a member of volume Bragg gratings (VBGs), is a functional planar structure with a patterned orientation of optical axis. Due to the strong polarization selectivity, nearly 100% diffraction efficiency, large diffraction angle, and simple fabrication process, PVGs have found potential applications in novel photonic devices and emerging near-eye displays. In this work, we start from the operation principles and liquid crystal configurations to discuss the optical properties, including diffraction efficiency, angular and spectral response, and polarization state of the diffracted light. Specifically, we emphasize promising applications of PVGs for near-eye displays and novel photonic devices. Through analyzing the functionalities of PVGs with simulations, PVG-based novel devices are proposed. We further develop polarization volume lenses (PVLs) with high diffraction efficiency, low *f*/#, and large diffraction angles. Previously reported planar lenses are of thin form factor but with on-axis imaging and large *f*/#. By patterning PVGs with parabolic phase, the obtained PVLs exhibit a small *f*/#, high diffraction efficiency, and large off-axis diffraction angle. The PVLs offer a new design for near-eye systems, especially for augmented reality (AR) displays. Based on PVLs, we propose a new multi-focal-plane AR system with a polarization multiplexing method to eliminate the vergence-accommodation conflict.

Keywords: polarization volume gratings, augmented reality displays, liquid crystals.

1. INTRODUCTION

Polarization volume gratings (PVGs) based on patterned cholesteric liquid crystals (CLC) have attracted increasing attention in both liquid crystal and photonics fields [1-3]. Ascribed to its intriguing formation process and distinct optical properties, PVG is particularly useful for novel optical devices and emerging displays, such as near-eye optical systems [4,5]. As a branch of Bragg gratings [6], PVGs with high efficiency, large diffraction angle, and strong polarization selectivity, shed new light on a unique molecular orientation profile [2,7,8]. Following two-dimensional patterned alignment, the chiral molecules promote the self-organization of bulk LC and then an asymmetric helical structure is formed. Compared to conventional Bragg gratings, such as holographic volume gratings (HVGs) [9,10], PVGs achieve nearly 100% diffraction efficiency at a very large diffraction angle, moreover, it possesses a wider angular response to incident light. In addition to distinctive optical functions, PVGs also exhibit attractive features such as elasticity [11,12], thermal and electrical responses [13], etc. Besides optical field, this CLC structure with the circularly polarized response is also surprisingly similar to the helical architecture of insects in nature, such as beetles [14]. In recent years after in-depth studies, a deeper understanding on the operation principles and characteristics of PVGs have been achieved [15]. Moreover, various PVG-based applications are emerging, such as beam steering, near-eye optical systems, head-up displays, and so on [16-19].

In this paper, we review recent advances of LC-based PVGs and propose some novel devices and systems based on this fascinating optical component. Here, we begin with LC director configuration to reveal the operation principles of PVGs. Then we dive into the model and characterize the unique optical properties through simulation results. Next, the fabrication process including molecular alignment method and exposure system is discussed. Finally, we introduce the applications of PVGs in emerging near-eye display systems, especially for augmented reality (AR).

Advances in Display Technologies XI, edited by Jiun-Haw Lee, Qiong-Hua Wang,
Tae-Hoon Yoon, Proc. of SPIE Vol. 11708, 1170804 · © 2021 SPIE · CCC
code: 0277-786X/21/$21 · doi: 10.1117/12.2577992

2. OPERATION PRINCIPLES AND PROPERTIES

2.1 Operation Principles

Before we discuss the physical principles, we need to know the internal structure of PVGs. Interestingly, with further research on physical models and experiments, the understanding of the LC director configuration in PVGs have experienced a transition. At first, the bulk structure was thought to be planar as Figure 1(a) depicts, where all the LC directors are parallel to the substrate [2,7,8]. The helical axis of CLC is perpendicular to the substrate and the CLC structure rotates following the bottom sinusoidal alignment pattern. This configuration produces an overall Bragg structure with Bragg pitch obeying following equation:

$$\frac{1}{P_G^2} = \frac{1}{P_x^2} + \frac{1}{P_z^2}, \tag{1}$$

where P_z in this case is equal to the CLC pitch P_{CLC}. This presumed planar structure accords with our intuition in that all the LC directors follow the bottom planar alignment perfectly. Besides, like the geometric phase (or Pancharatnam-Berry phase) in transmissive LC polarization gratings [20-22], it also exists in reflective CLC structures [23]. The rotation of the helical axis, therefore, generates the geometric phase that can be utilized to fabricate various optical elements [2]. So far, the planar structure explains some experimental results well.

Nonetheless, it has been pointed out [15] that the bulk structure in a planar-PVG is not in the most relaxed state (pure helix structure), which is reflected in its free energy density (single-constant approximation):

$$f = \frac{K}{2}\left[(\nabla \cdot n)^2 + (n \cdot \nabla \times n + \frac{2\pi}{P_{CLC}})^2 + \left| n \times \nabla \times n \right|^2 \right], \tag{2}$$

$$f_{planar} = \frac{K}{2}\left(\frac{2\pi}{P_x} \right)^2. \tag{3}$$

From Equation 3, the bulk free energy density of the planar structure is non-zero and inversely proportional to $(P_x)^2$. The effect of the deviation from perfectly relaxed state is not obvious when P_x is relatively large (much larger than the pitch of CLC) [2]. However, as the deflection angle of PVG gets larger, P_x eventually evolves into a small value comparable to the CLC pitch length. In this case, the bulk free energy is so high that the system becomes unstable.

Recently, some experiments on the polarization response in PVG indicate that the bulk structure may be in a slanted configuration [24]. This issue is explicitly explained in [15] through simulation and experimental validation. The slanted PVG, as shown in Figure 1(b), preserves the perfect helical structure in the bulk, which results in its lowest free energy (the bulk free energy is zero). The Bragg pitch PG in this case is equal to the CLC pitch P_{CLC}. The bottom alignment gives the bulk helical structure a tilt angle $\alpha=\arcsin(P_G/P_X)$ to match the bottom k-vector with the bulk periodic structure. To transit from the bottom planar alignment to the bulk slanted structure, there exists a transitional region (red box in Figure 1(b)) with non-zero free energy. However, the thickness of this transitional region is usually very small (tens of nanometers), so its contribution to the total free energy is minor. Therefore, the large-angle PVG formed by one-time spin coating or cell formation manifests the slanted structure.

As discussed in [15], the formation of planar-PVGs requires: 1) large P_x (where planar-PVGs and slanted-PVGs are indistinguishable), or 2) strong anchoring and small thickness (less than 300 nm for each layer, and multiple spin-coatings to gain sufficient thickness, about 3 μm). At the same time, except polarization selectivity (which we will discuss later), the optical properties of planar-PVGs and slanted-PVGs are very similar in terms of reflection efficiency, wavelength response, and angular response. Therefore, from the perspective of practical application, the slanted-PVGs formed by one-time assembly is more advantageous. For the convenience of discussion, unless otherwise mentioned, the PVG we refer to is the slanted one.

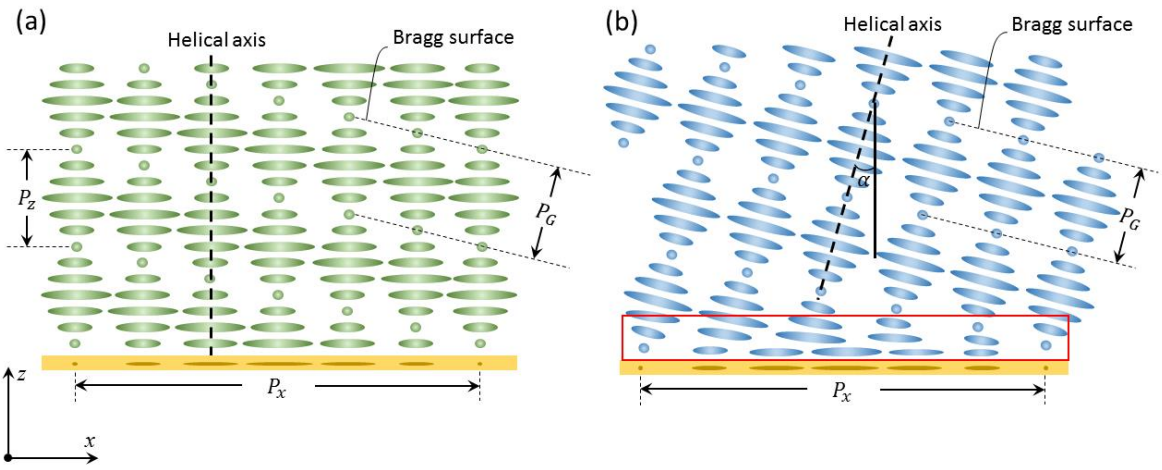

Figure 1. Different LC director configurations of PVG. (a) Planar-PVG with helical axis perpendicular to substrate surface. (b) Slanted-PVG with helical axis perpendicular to Bragg surface. The red box indicates the transitional region from planar to slanted structure.

2.2 Optical Properties

To comprehensively show the diffractive properties of PVGs, we have built a rigorous simulation model using commercial Finite Element Method (FEM) package. For PVGs, there are several important characteristics that deserve special attention, including: diffraction efficiency, wavelength response, angular response, and polarization response. As shown in Figure 2(a), only circularly polarized light with the same handedness as the helical rotation will be diffracted (in this case, right-handed circular polarization RCP), while the opposite handedness (LCP) will pass through. Besides, as Bragg volume gratings, the PVGs should be thick enough to establish Bragg diffraction. As depicted in Figure 2(b), the diffraction efficiency is directly related to the film thickness.

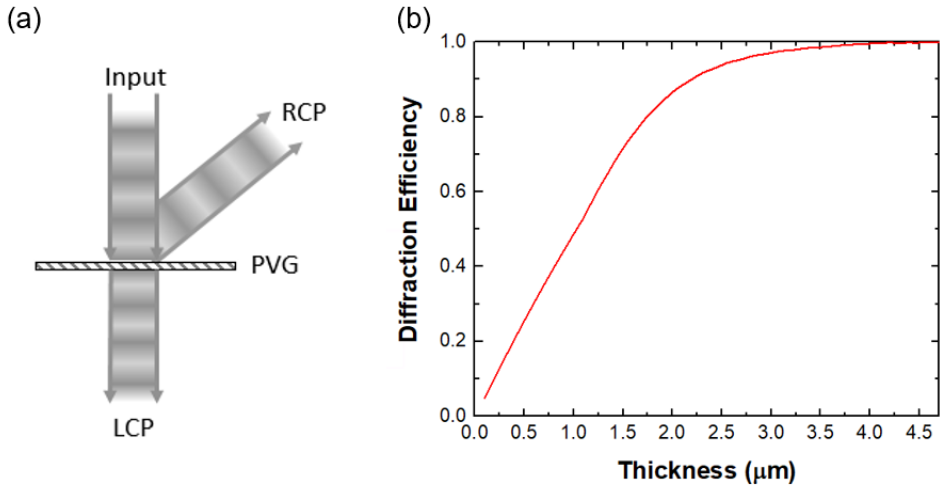

Figure 2. (a) Schematic of the beam diffracted by a PVG. (b) Simulated diffraction efficiency as a function of film thickness. The diffraction efficiency is defined as the ratio of first-order diffracted light to incident light at a specific diffraction angle and center wavelength. The horizontal period is 440 nm, vertical period is 205 nm, Δn=0.15, the diffraction angle is 50°, and the central wavelength is 532 nm. The efficiency is higher than 95% when the thickness exceeds 3 μm.

As the thickness increases, diffraction efficiency grows monotonically at the beginning and then gradually saturates and approaches 100%. Therefore, for a certain wavelength, the required thickness for achieving high diffraction efficiency can be easily obtained based on the number of pitches. Compared to a conventional volume holographic grating whose

thickness is at least tens of micrometers, PVG (several micrometers) is much thinner. Besides, it is important to note that the efficiency is only for a circularly polarized input and the opposite circular polarization can fully transmit through the PVG. This feature provides high transmittance for the ambient light, which is important for see-through near-eye displays.

As analyzed in Section 2.1, the Bragg diffraction of PVGs is based on the helical twist along the LC optical axis. Therefore, the effective index modulation in PVGs is essentially the birefringence of the LC material. Due to the matured LCD industry, a wide range of birefringence (Δn=0.05 to 0.4) is available. Same as the spectral properties of CLC, the reflection band of PVGs could be easily tuned by using a LC with different Δn, as Figure 3(a) depicts. Usually, as Δn increases, the reflection band gets wider. Furthermore, Figure 3(b) shows the diffraction efficiency spectra at three different diffraction angles with Δn of 0.15. From these simulation results, we can see that the diffraction efficiency and bandwidth are almost independent of diffraction angle. This means the PVGs can diffract light to different angles while keeping high efficiency, which is a very favorable feature for near-eye display systems.

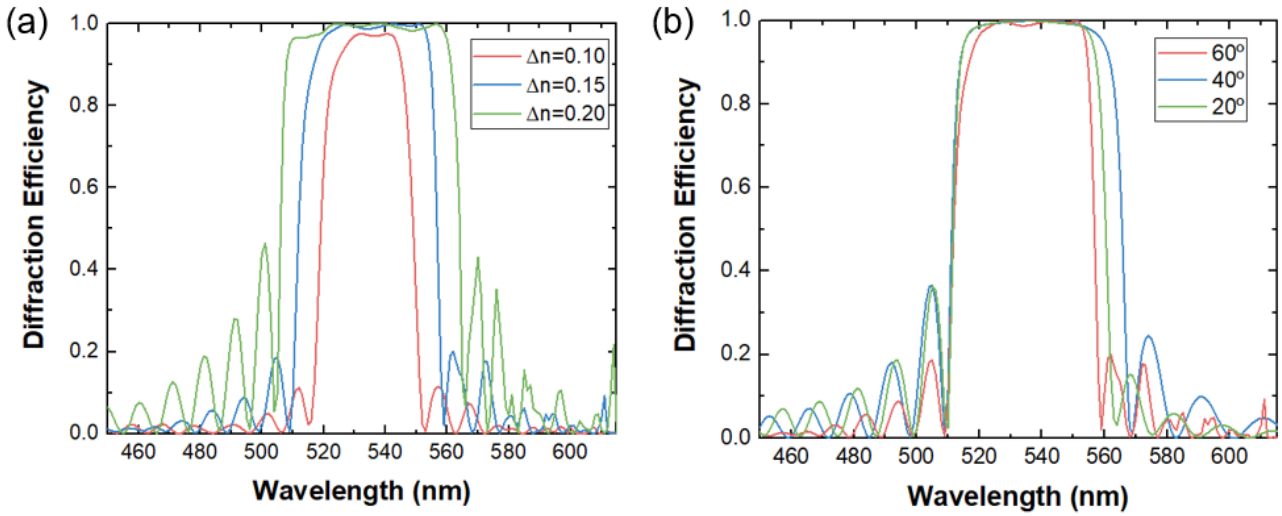

Figure 3. Wavelength response of PVGs. (a) Diffraction efficiency spectra at normal incidence and 50° diffraction angle with different refractive index contrast and (b) different diffraction angles with Δn = 0.15.

Not only diffraction spectrum, the angular selectivity is also closely related to Δn. Thus, the angular response via different birefringence is investigated and illustrated in Figure 4(a). The angular band of incident light becomes broader as Δn increases. Compared to the effective index modulation in holographic volume grating (typically of the order of 10^{-2}), the LC birefringence is much higher (typically 0.15). As a result, the PVG possesses a wider angular bandwidth, which is much needed in many applications, such as light couplers in near-eye systems. These will be discussed later. Besides, it is worth mentioning that the angular response is sensitive to diffraction angle as well. Figure 4(b) shows the angular bandwidth for different diffraction angles with the same Δn (0.15). The trend is clear: as the diffraction angle increases, the angular band of incident light for achieving high diffraction efficiency is broader.

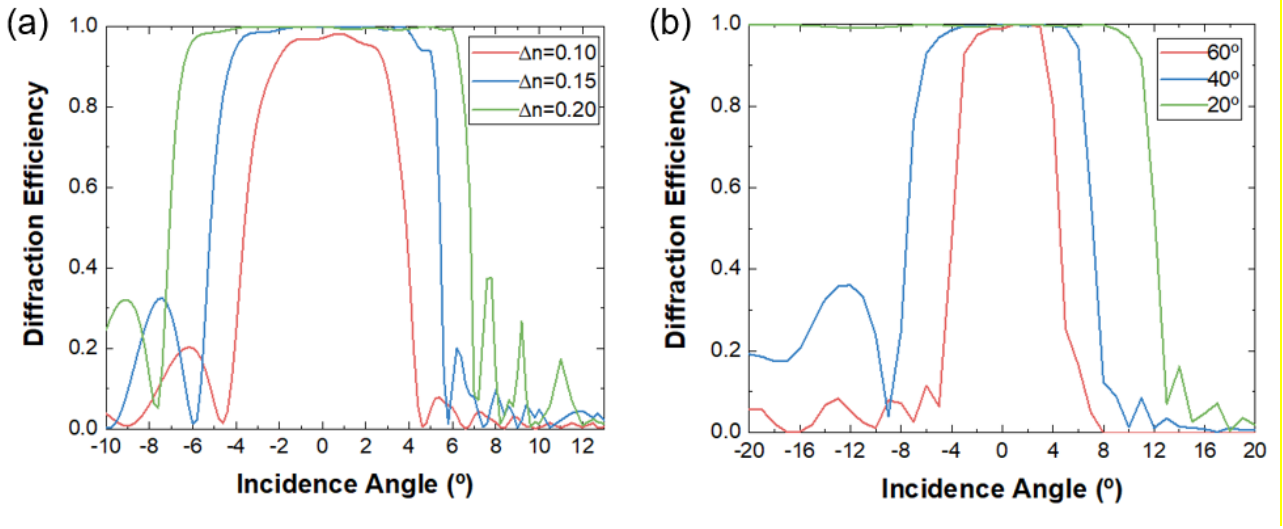

Figure 4. Angular response of PVGs. (a) Diffraction efficiency versus incident angle at three refractive index contrasts with 50° diffraction angle and (b) three diffraction angles with $\Delta n = 0.15$.

In addition to spectral and angular responses of PVGs, polarization response is another unique property. This part is rarely discussed in previous reports, but the study of polarization properties is necessary for PVGs to be used in cascaded optical systems where polarization control is pivotal. In an early study, it was described that the first order diffracted light maintains a circular polarization with an appropriate input circular polarization [7]. Specifically, the input circularly polarized light will keep its handedness or flip its handedness when diffracted by a reflective or transmissive PVGs. Later, Xiang et al. fabricated transmissive PVGs and surprisingly, the polarization state of the first order deviates severely from circular polarization [25], which was further proven in their simulation work [26]. Recently, Lee et al. analyzed the polarization response of reflective PVGs [24]. Numerical analysis shows that for the traditional planar configuration (Figure 1(a)), the polarization of the first order diffracted light deviates from circular polarization, which agrees with that reported in [26]. However, in experiment, the measured polarization state of the first order is highly circular (Stokes parameter S3 ~ 1). To explain this, the slanted configuration of PVG (Figure 1(b)) was proposed [24]. In a traditional planar PVG, the helical axis of cholesteric liquid crystals is oriented at the vertical axis, while in the slanted configuration, the helical axis is perpendicular to the Bragg planes.

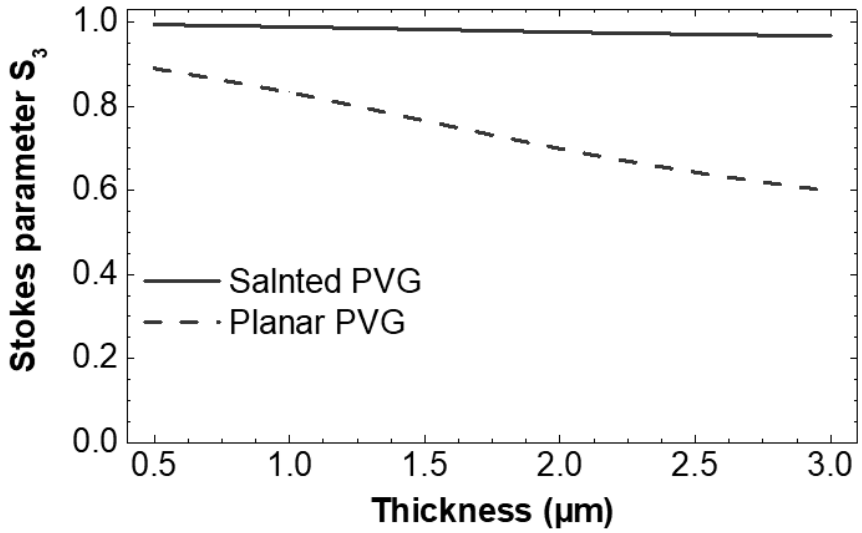

Figure 5. Stokes parameters S3 as a function of film thickness. The horizontal period (P_x) is 440 nm, vertical period (P_z) is 205 nm, central wavelength is 532 nm and Δn is 0.15.

To investigate the polarization property of the diffracted light, we use Stokes parameter S3 as an indicator. S3 denotes the degree of circular polarization of light. For example, S3=1 means RCP light, while S3=−1 stands for LCP light. In the simulation, the horizontal period (P_x) is 440 nm and vertical period (P_z) is 205 nm, which results in a slanted angle of α=25°. The central wavelength is set at 532 nm, and Δn is 0.15. At normal incidence, the first-order polarization state of the slanted configuration is very close to circular polarization, as shown in Figure 5. By contrast, the diffracted light from the planar PVG significantly deviates from circular polarization.

The previous investigation in polarization response seeded the finding of slanted configuration of PVGs. Nevertheless, the study of polarization response is merely a starting point. Both slant angle and incident angle make significant impacts on the polarization response. Further detailed analysis is necessary to understand its optical response.

3. DEVICE FABRICATION

In addition to unique optical characteristics, simple fabrication process is another noteworthy advantage of PVGs. Since PVGs are essentially a grating based on liquid crystal, recording high-quality patterns to align liquid crystal molecules is an important step during fabrication. Compared to conventional rubbing method [27], photo-alignment is a more advantageous option for generating precise patterns [28-30].

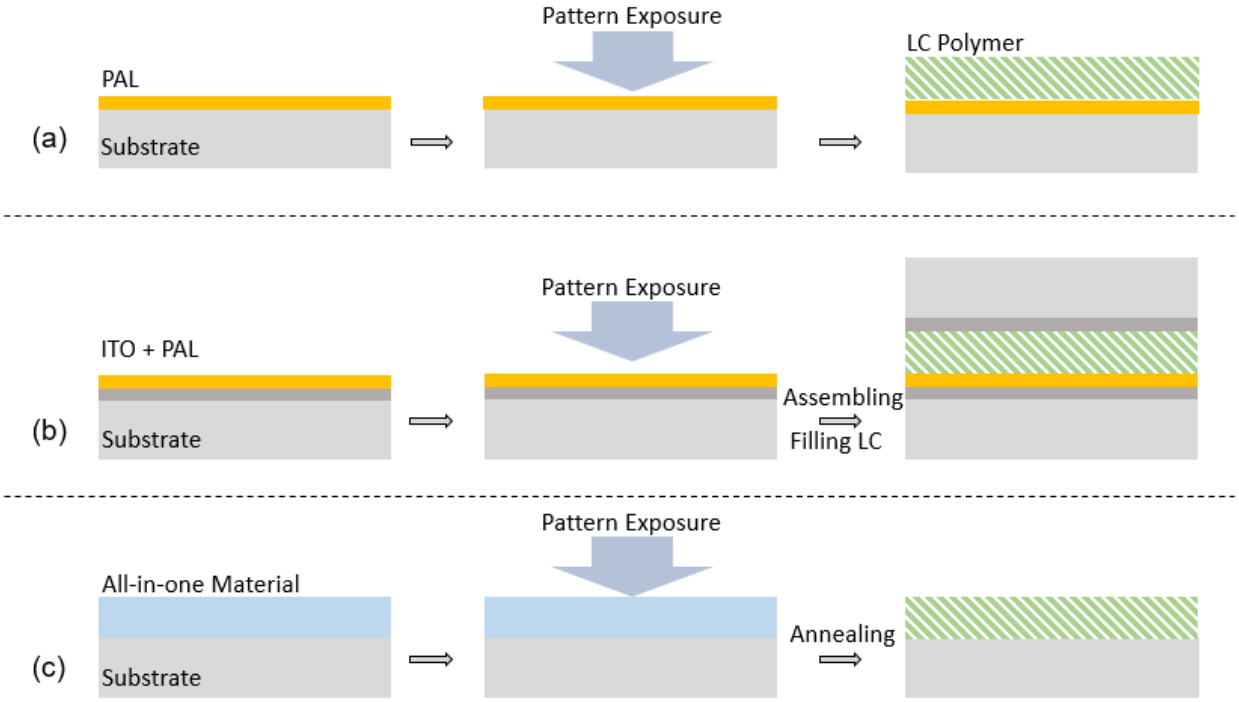

Figure 6. Fabrication procedures of PVGs. (a) Surface alignment for LC polymeric PVG. (b) Electrically responsive LC PVG. (c) Volume alignment.

3.1 Liquid Crystal Alignment

Two approaches have been widely used in the fabrication based on photo-alignment materials. The first approach is surface alignment, which utilizes polarization interference to pattern a thin photo-alignment layer (PAL) [31-35]. The subsequently coated or sprayed liquid crystals self-align into gratings following the recorded patterned surface. To fabricate a polymeric PVG film, the LC precursor typically contains LC monomer, solvent, photo-initiator, and surfactant [36,37]. After the alignment process, we expose the sample with ultra-violet light (λ=365 nm, room temperature, 10 mW/cm^2 for 5 minutes) to polymerize the film. By contrast, to fabricate an electrically switchable PVG, two thin PAL-coated ITO glass substrates are assembled to form a uniform cell. After recording the alignment, we inject LC to the cell at an isotropic phase

temperature [38] and let it cool down to the room temperature. Then diffraction behavior of the PVG can be tuned by applying a voltage [14]. Surface alignment is the most established method so far for PVGs fabrication, as Figures 6(a) and 6(b) depict. The second approach is to record the volumetric polarization field by applying the photocycloaddition of cinnamate groups or similar all-in-one materials [39-41]. After the bulk LC alignment, the film is annealed to induce birefringence. This process is illustrated in Figure 6(c).

3.2 Exposure System

The polarization field used to provide LC orientations is usually generated by light exposure [42-44]. In the simplest case, the grating can be formed by a polarization interferometer, shown in Figure 7(a). The linearly polarized laser beam is filtered and expanded, then split into two arms by a beam splitter (BS). A quarter-wave plate is placed in each arm to convert the incident light to RCP (Path 1) and LCP (Path 2). Then these two beams are reflected by the mirrors (M) to interfere at the sample (S). Normally, the PVG phase can be obtained without other optical components in box A. However, appropriate modifications can be made to achieve exotic PVG phase profiles. For example, if a cylindrical lens is added, then the polarization filed has an additional parabolic phase in one dimension, so that the fabricated PVG shows a period of gradient change according to the direction of the cylindrical lens. In addition, if a lens is added, then the final PVG would have an additional parabolic phase profile in two dimensions, which makes it no longer a grating, but a polarization volume lens.

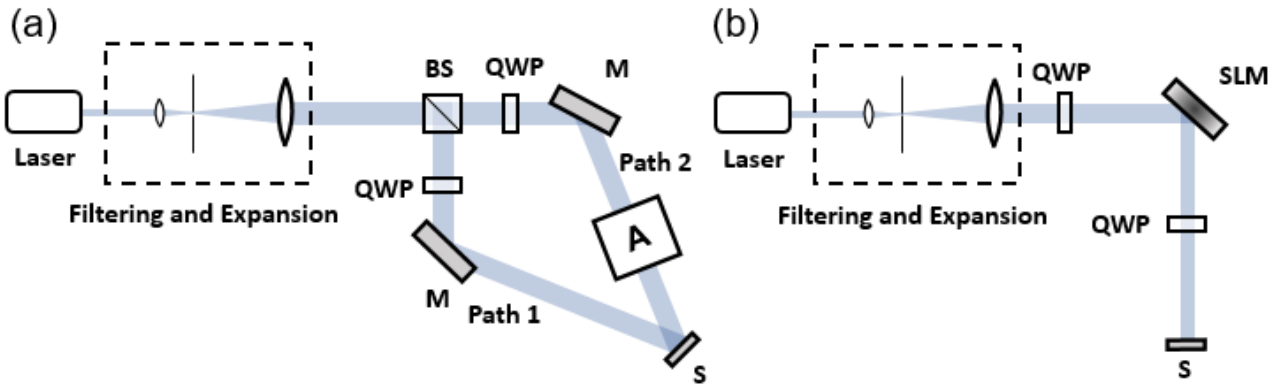

Figure 7. Exposure setups of PVGs. (a) Two-beam interferometer. (b) Exposure based on SLM.

Besides, the polarized light field for fabricating PVGs can also come from a pixelated spatial light modulator (SLM) [45-47]. As depicted in Figure 7(b), the collimated linearly polarized laser beam is converted to circular polarization by a QWP, and then is reflected by a high resolution SLM. The spatially modulated laser beam is changed back to linear polarization by the second QWP and imaged onto the substrate coated with the photo alignment material. The resolution of this method is limited by the pixel density of the SLM. If the period is too small to record, then a lens-system needs to be added to compress the pattern to meet the requirements. Although this method has some limitations, it still provides a possible solution for fabricating PVGs and other PVG-based devices with designed patterns [48].

4. NEAR-EYE DISPLAYS

Besides novel optical elements, the unique properties of PVGs also open new space in near-eye displays, especially novel optical systems for augmented reality (AR) displays. At current stage, there are still many unresolved challenges in near-eye display systems, such as expanding field of view (FOV), increasing the system efficiency, generating more depths to decrease the dazzling, and improving the uniformity of image [49, 50]. The combination of PVGs and new optical systems offers intriguing solutions for near-eye displays [4].

4.1 Waveguide-based AR Display Coupler

The basic construction of a waveguide-based AR display includes a display panel as image source, magnifying optics, and couplers to overlay computer generated images and real world. Normally, the light that comes from the display is first

guided into a thin glass plate (the “waveguide”) by the input grating coupler, and then propagates inside the waveguide due to total internal reflection (TIR). An output coupler is placed at the see-through area to extract the light out of the waveguide and toward the human eye. As a critical component in this system, the grating coupler must meet the following conditions: large diffraction angle (to generate TIR), high single-order diffraction efficiency, and decent angular response (to support the required FOV). As we analyzed in Section 3, PVG meets these requirements and is therefore very suitable as coupler for waveguide-based AR displays.

Although both transmissive and reflective PVGs could be used as the input coupler, the reflective type shows a wider angular response bandwidth under the same average index [26]. Different from the input coupler, the output coupler has 3 important functions: 1) to export light from the waveguide to the human eye, 2) to achieve good uniformity of the outgoing light, and 3) to ensure an eye-box with decent size in both lateral and vertical directions. As a result, the output coupler with pupil dilation function is usually called exit pupil expander (EPE). A typical method for expanding the exit pupil is to use an output coupler with gradient diffraction efficiency. As the beam passing through the waveguide, its intensity decreases when it encounters the output coupler. This gradient-efficiency approach has been well developed in commercial AR products with holographic volume gratings or surface relief gratings [19]. Since the diffraction efficiency of PVGs is closely related to the thickness of the film, the gradient-efficiency can be achieved by controlling the thickness. Therefore, the gradient-efficiency method is also applicable to waveguides using PVG couplers, as Figure 8(a) illustrates [51,52].

Because the diffraction efficiency of PVGs is also highly sensitive to the input polarization state, another approach based on polarization management layer (PML) can also be utilized for expanding the exit light [4, 19]. As Figure 8(b) shows, instead of generating gradient diffraction efficiency, a PML is added on the PVG-based waveguide to boost the efficiency and distribute the output light. In such design, the PML is essentially a transparent LC film that has different azimuthal angles at different locations to control the polarization state. Each time the light passes through the PML, the polarization state is adjusted so that the required amount of light is coupled out during the next interaction with the output coupler. By designing the film thickness and the azimuthal angle of the LC in the PML, good uniformity of the output intensity along the entire out-coupling region can be achieved. Moreover, in comparison with the gradient-efficiency method, this PML approach can provide a relatively uniform ambient light transmittance, thereby avoiding clearly visible segment regions in the EPE area.

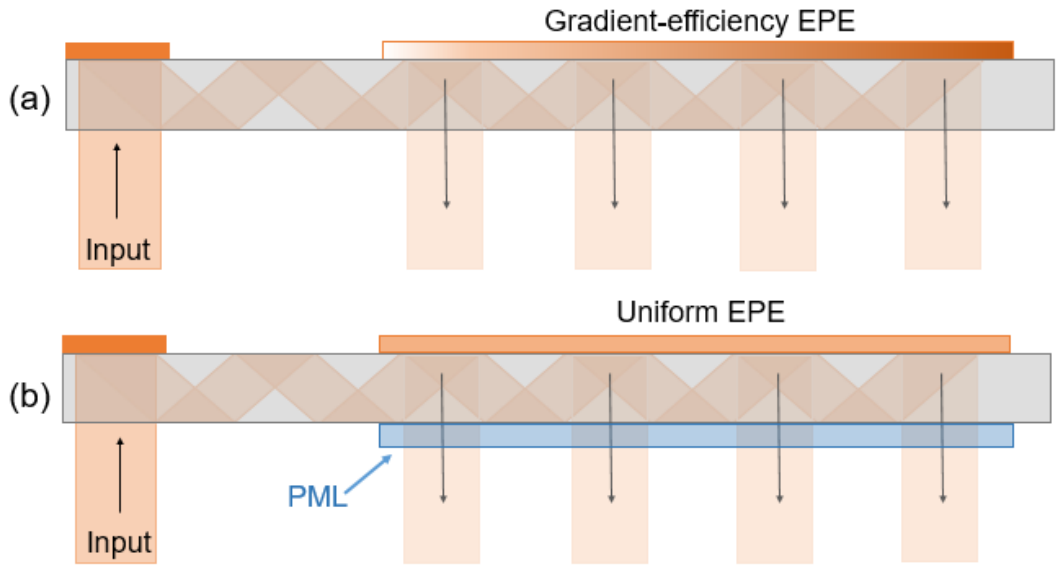

Figure 8. Schematic illustration of waveguide-based optical systems. (a) Using gradient-efficiency output coupler. (b) Using uniform-efficiency output coupler with a PML.

4.2 Wide Field of View

In most waveguide-based AR systems, the FOV is highly dependent on the angular response of the coupler and is limited by the TIR of the waveguide itself. In order to expand the FOV of the system, we can tackle two aspects: 1) using a high index glass to extend the TIR limit, and 2) increasing the angular response of the couplers. To broaden the angular response,

some designs based on the vertical twist structures [53,54] have been developed for both reflective and transmissive PVGs. Previously, a two-layer twisted transmissive PVG was designed, in which each layer is a transmissive PVG with the same deflection angle but different slanted angles. This method is effective, but the diffraction efficiency is not as high as expected. As reported in [53], the measured angular bandwidth is 40º and the average diffraction efficiency within the band is about 30%. More recently, for reflective PVGs, a gradient-pitch method [54] was proposed and fabricated to dramatically widen the angular bandwidth [55]. By inducing a gradually changing period along the vertical direction while the period along the horizontal direction is fixed, a wider angular bandwidth can be obtained. Figure 9(a) shows the device structure of this gradient-pitch PVG. The fabrication procedure of such a gradient-pitch grating is similar to that described in Section 3, except for different precursors and UV curing conditions. Compared to previous mixture (LC monomers, solvents, photo-initiators, and surfactants), we added a 1.50-wt% UV dye (Avobenzone) to help generate gradually changing period, and then raised the curing temperature to 60 °C and cured with a low power ultraviolet light (λ=365 nm, 0.3 mW/cm^2) for 40 minutes. Figure 9(b) shows the simulated and measured angular responses and a photo of the sample. In experiment, the angular bandwidth is extended to 54° while keeping an over 80% diffraction efficiency. Such a wide FOV enables PVGs to become a strong contender for AR displays [18].

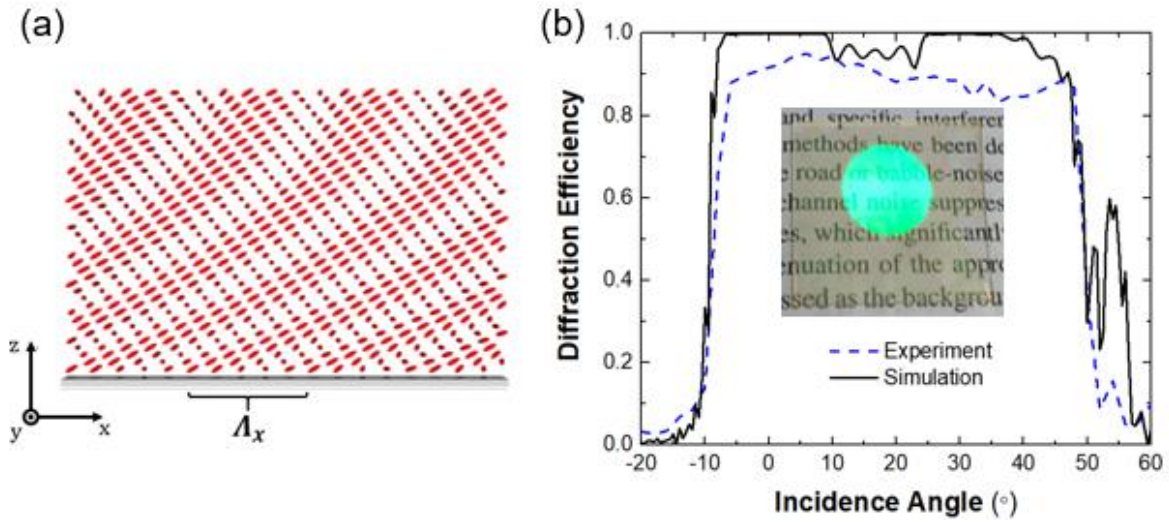

Figure 9. (a) Schematic diagram of gradient-pitch PVG. (b) Simulation and experimental results of angular response. Inset: photo of the sample.

We used a micro-OLED as the image source to build an AR optical system. Figure 10(a) is a picture of our AR prototype [18]. Here we combine a micro-OLED with a lens to generate collimated input image. Figure 10(b) shows the experimental results. We send a green "A" as the input image into the assembled AR device and then take picture at output. The coupled-out image is quite uniform but a little blur. Because when the light propagating in the waveguide (glass slab), the TIR may occur at or near to the edge of the CPVG substrate. Therefore, the light is scattered by the rough surface of the glass edge. Such a rough edge is caused by our laboratory fabrication equipment and can be eliminated by better assembly method in the future. Besides, the optical glue that we used to assemble the module will also accumulate at the edge and scatter the light. In general, the results show the feasibility of our CPVG for AR systems. Although the output image is slightly hazy and the background is not bright enough, the prototype still shows good performance.

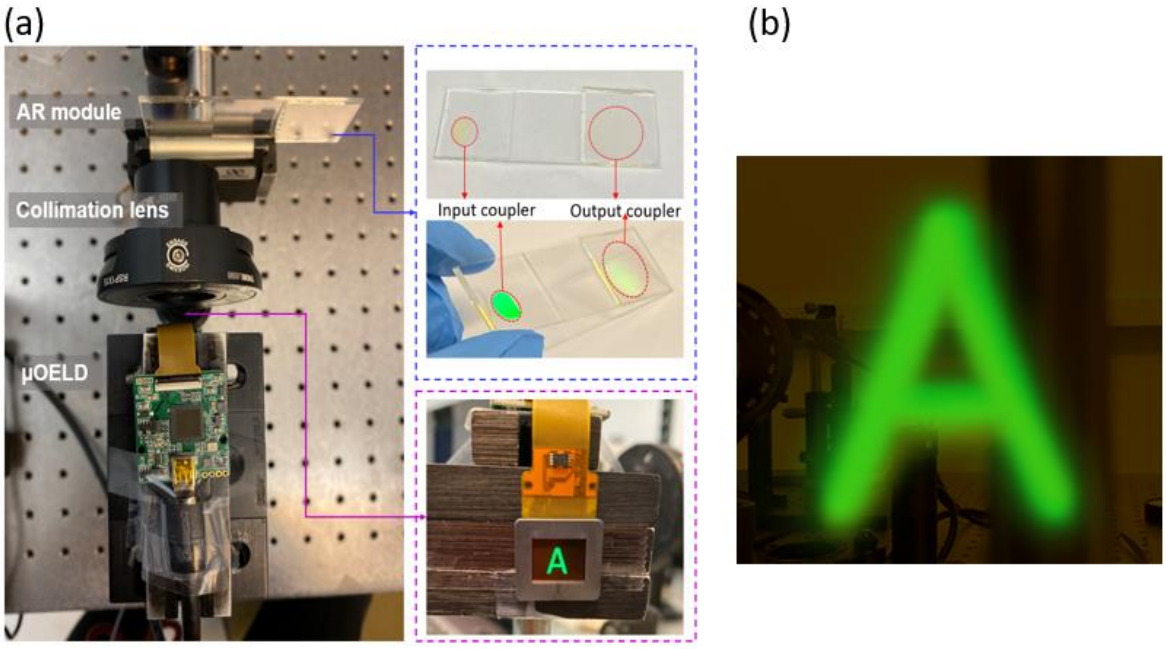

Figure 10. (a) Picture of an AR prototype, including a micro-OLED panel and two CPVGs. (b) Photo of the output image. [18]

4.3 Polarization Volume Lens (PVL)

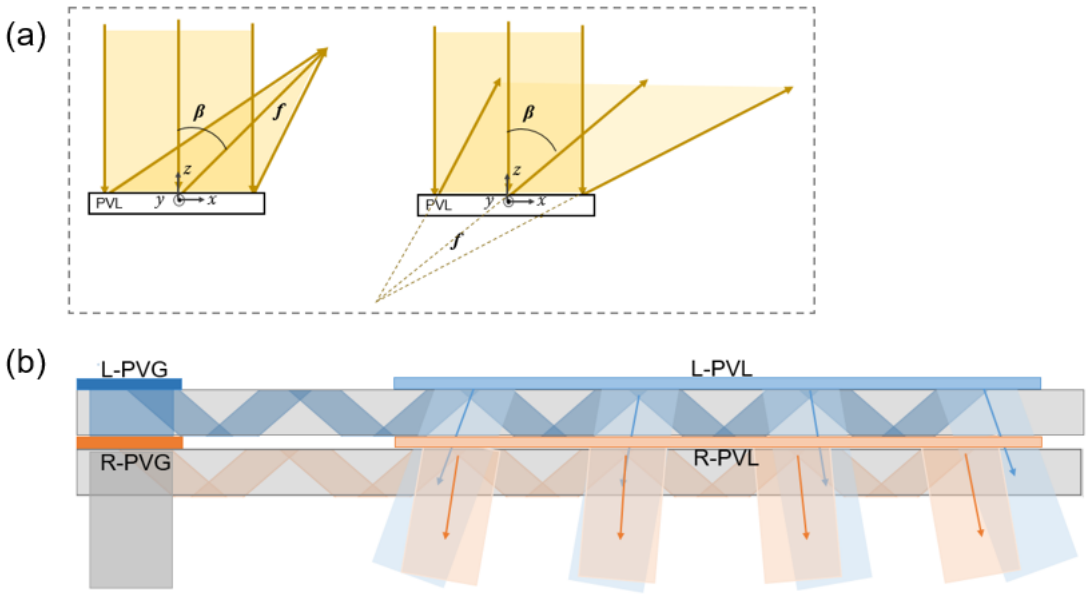

Figure 11. (a) Schematic diagram of PVL, (b) Schematic illustration of two-focal-plane waveguide-based AR system.

As a coupler with high efficiency and large deflection angle, PVGs have shown promising applications to AR optical systems. However, for certain situations, such as multi-focal plane designs, it requires components with more features than regular gratings, for example, a lens. Fortunately, it is possible to further implement the lens function on the basis of PVGs.

If a lens is added into the exposure setting as a template, then the final PVG would have an additional parabolic phase profile, which makes it a polarization volume lens (PVL) [2]. The operation principle of PVL is equivalent to combining a reflective PVG with a lens. Such a PVL is useful as an off-axis mirror for converging or diverging the incident light; the incident light is focused/diversified by the lens profile and diffracted by the grating. Recently, a PVL with small f-number and large diffraction angle has been reported [56] that provides a solid theoretical foundation and a promising fabrication process. Figure 11(a) illustrates the schematic diagram of the PVL.

Next, let us go back to the AR system. Due to the limited focal planes, one of the major challenges for near-eye displays is the vergence-accommodation conflict (VAC) [57,58]. To overcome the VAC issue, several methods have been proposed, such as multi-focal-plane displays [59], light field displays [60,61], and holographic displays [62,63]. Here, we propose a two-focal-plane system with PVL for waveguide-based AR displays. Figure 11(b) depicts the system configuration. This design has a stacked two-layer structure, which has been widely used in commercial products. The light beams carrying different polarization information (LCP and RCP) are respectively coupled into different two-layer waveguides through two counter-twist PVGs. Due to the TIR, the light propagates inside the glass slab and reaches the output areas. Here two PVLs with opposite polarization responses (LCP and RCP) and different diopters are used as output couplers to extract light toward the human eye. Based on this simple but effective design, the image contents with different polarization states are projected to different depths.

5. SUMMARY

In summary, PVGs are novel optical elements based on patterned liquid crystal structures. They exhibit high diffraction efficiency, large diffraction angle, thin-film form factor, and strong polarization selectivity. By replacing the surface alignment pattern, we obtain the PVL with off-axis and designed lens power. These novel optical elements shed new light on the AR system. The high-efficiency PVGs can be applied as the coupler, especially for the waveguide-based near displays. It is worth mentioning that the FOV and the VAC are still the challenges in the AR system. Therefore, to address these issues, we propose the chirped PVG with gradient pitch to enlarge the viewing angle of the grating. Besides, we propose the two-focal system with the PVL to mitigate the VAC in the waveguide AR system. Due to the unique optical properties and ultra-thin form factor, both PVGs and PVLs show promising applications in the AR system.

REFERENCES

1. Barboza, R., Bortolozzo, U., Clerc, M.G. and Residori, S., "Berry phase of light under Bragg reflection by chiral liquid-crystal media," Phys. Rev. Lett. 117, 053903 (2016).
2. Kobashi, J., Yoshida, H. and Ozaki, M., "Planar optics with patterned chiral liquid crystals," Nat. Photonics 10, 389 (2016).
3. Kobashi, J., Mohri, Y., Yoshida, H. and Ozaki, M., "Circularly-polarized, large-angle reflective deflectors based on periodically patterned cholesteric liquid crystals," Opt. Data Process. Storage 3, 61–66 (2017).
4. Lee, Y.H., Zhan, T. and Wu, S.T., "Prospects and challenges in augmented reality displays," VRIH 1, 10-20 (2019).
5. Zhan, T., Lee, Y.H., Tan, G., Xiong, J., Yin, K., Gou, F., Zou, J., Zhang, N., Zhao, D., Yang, J., Liu, S. and Wu, S.T., "Pancharatnam-Berry optical elements for head-up and near-eye displays," J. Opt. Soc. America B 36, D52-D65 (2019).
6. Gaylord, T.K. and Moharam, M.G., "Thin and thick gratings: terminology clarification," Appl. Opt. 20, 3271-3273 (1981).
7. Weng, Y., Xu, D., Zhang, Y., Li, X. and Wu, S.T., "Polarization volume grating with high efficiency and large diffraction angle," Opt. Express 24, 17746-17759 (2016).
8. Lee, Y.H., Yin, K. and Wu, S.T., "Reflective polarization volume gratings for high efficiency waveguide-coupling augmented reality displays," Opt. Express 25, 27008-27014 (2017).
9. Rasmussen, T. "Overview of high-efficiency transmission gratings for molecular spectroscopy," Spectroscopy 29, 32-39 (2014).

10. Moharam, M.G., Grann, E.B., Pommet, D.A. and Gaylord, T.K., "Formulation for stable and efficient implementation of the rigorous coupled-wave analysis of binary gratings," J. Opt. Soc. Am. A 12, 1068-1076 (1995).
11. Yin, K., Lee, Y.H., He, Z. and Wu, S.T., "Stretchable, flexible, and adherable polarization volume grating film for waveguide-based augmented reality displays," J. Soc. Inf. Disp. 27, 232-237 (2019).
12. Yin, K., Lee, Y.H., He, Z. and Wu, S.T., "Stretchable, flexible, rollable, and adherable polarization volume grating film," Opt. Express 27, 5814-5823 (2019).
13. Chen, R., Lee, Y.H., Zhan, T., Yin, K., An, Z. and Wu, S.T., "Multistimuli-responsive self-organized liquid crystal Bragg gratings," Adv. Opt. Mater. *7*, 1900101 (2019).
14. McDonald, L. T., Finlayson, E. D., Wilts, B. D. and Vukusic, P., "Circularly polarized reflection from the scarab beetle Chalcothea smaragdina: light scattering by a dual photonic structure," Interface Focus 7, 20160129 (2017).
15. Xiong, J., Chen, R. and Wu, S.T., "Device simulation of liquid crystal polarization gratings," Opt. Express 27, 18102-18112 (2019).
16. Zhan, T., Lee, Y.H., Xiong, J., Tan, G., Yin, K, Yang, J., Liu, S. and Wu, S.T., "High-efficiency switchable optical elements for advanced head-up displays," J. Soc. Inf. Disp. 27, 223-231 (2019).
17. He, Z., Gou, F., Chen, R., Yin, K., Zhan, T. and Wu, S.T., "Liquid Crystal Beam Steering Devices: Principles, Recent Advances, and Future Developments," Crystals 9, 292 (2019).
18. Yin, K., Lin, H.Y. and Wu, S.T., "Chirped polarization volume grating for wide FOV and high efficiency waveguide-based AR displays," J. Soc. Inf. Disp. 28, 368-374 (2020).
19. Lee, Y.H., Tan, G., Yin, K., Zhan, T. and Wu, S.T., "Compact see-through near-eye display with depth adaption," J. Soc. Inf. Disp. 26, 64-70 (2018).
20. Tabiryan, N.V., Serak, S.V., Roberts, D.E., Steeves, D.M. and Kimball, B.R., "Thin waveplate lenses of switchable focal length-new generation in optics," Opt. Express 23, 25783-25794 (2015).
21. McManamon, P.F., Bos, P.J., Escuti, M.J., Heikenfeld, J., Serati, S., Xie, H. and Watson, E. A., "A review of phased array steering for narrow-band electrooptical systems," Proc. IEEE 97, 1078-1096 (2009).
22. Lee, Y.H., Tan, G., Zhan, T., Weng, Y., Liu, G., Gou, F., Peng, F., Tabiryan, N.V., Gauza, S. and Wu, S.T., "Recent progress in Pancharatnam-Berry phase optical elements and the applications for virtual/augmented realities," Opt. Data Process. Storage 3, 79-88 (2017).
23. Barboza, R., Bortolozzo, U., Clerc, M.G. and Residori, S., "Berry phase of light under bragg reflection by chiral liquid-crystal media," Phys. Rev. Lett. 117, 053903 (2016).
24. Lee, Y.H., He, Z. and Wu, S.T., "Optical properties of reflective liquid crystal polarization volume gratings," J. Opt. Soc. Am. B 36, D9-D12 (2019).
25. Xiang, X., Kim, J., Komanduri, R. and Escuti, M.J., "Nanoscale liquid crystal polymer Bragg polarization gratings," Opt. Express 25, 19298-19308 (2017).
26. Xiang, X. and Escuti, M.J., "Numerical analysis of Bragg polarization gratings," J. Opt. Soc. Am. B 36, D1-D8 (2019).
27. Berreman, D.W., "Solid surface shape and the alignment of an adjacent nematic liquid crystal," Phys. Rev. Lett. 28, 1683-1686 (1972).
28. Gibbons, W.M., Shannon, P.J., Sun, S.T. and Swetlin, B.J., "Surface-mediated alignment of nematic liquid crystals with polarized laser light," Nature 351, 49-50(1991).
29. Schadt, M., Schmitt, K., V. Kozinkov, V. and Chigrinov, V., "Surface-induced parallel alignment of liquid crystals by linearly polymerized photopolymers," Jpn. J. Appl. Phys. 31, 2155-2164 (1992).
30. Ichimura, K., "Photoalignment of liquid-crystal systems," Chem. Rev. 100, 1847-1874 (2000).
31. Chigrinov, V., Muravski, A., Kwok, H.S., Takada, H., Akiyama, H. and Takatsu, H., "Anchoring properties of photoaligned azo-dye materials," Phys. Rev. E 68, 061702 (2003).
32. Tseng, M.C., Yaroshchuk, O., Bidna, T., Srivastava, A.K., Chigrinov, V. and Kwok, H.S., "Strengthening of liquid crystal photoalignment on azo dye films: passivation by reactive mesogens," RSC Adv. 6, 48181-48188 (2016).
33. Wang, J., McGinty, C., Reich, R., Finnemeyer, V., Clark, H., Berry, S. and Bos, P., "Process for a reactive monomer alignment layer for liquid crystals formed on an azodye sublayer," Materials 11, 1195 (2018).

34. Wang, J., McGinty, C., West, J., Bryant, D., Finnemeyer, V., Reich, R., Berry, S., Clark, H., Yaroshchuk, O. and Bos, P., "Effects of humidity and surface on photoalignment of brilliant yellow," Liq. Cryst. 44, 863-872 (2017).
35. Ouskova, E., Vergara, R., Hwang, J., Roberts, D., Steeves, D.M., Kimball, B.R. and Tabiryan, N., "Dual-function reversible/irreversible photoalignment material," J. Mol. Liq. 267, 205-211 (2018).
36. Decker C. and Moussa, K., "Real-time kinetic study of laser-induced polymerization," Macromolecules 22, 4455-4462 (1989).
37. Bryant, S.J., "Nuttelman, C.R., Anseth, K.S. Cytocompatibility of UV and visible light photoinitiating systems on cultured NIH/3T3 fibroblasts in vitro," J. Biomater. Sci. Polym. Ed. 11, 439-457 (2000).
38. Yang, D.K. and Wu, S.T., [Fundamentals of Liquid Crystal Devices], 2nd ed., John Wiley & Sons: Chichester, UK 161-169 (2014).
39. Sakhno, O., Gritsai, Y., Sahm, H. and Stumpe, J., "Fabrication and performance of efficient thin circular polarization gratings with Bragg properties using bulk photo-alignment of a liquid crystalline polymer," Appl. Phys. B 124, 52 (2018).
40. Emoto, A., Matsumoto, T., Yamashita, A., Shioda, T., Ono, H. and Kawatsuki, N., "Large birefringence and polarization holographic gratings formed in photocross-linkable polymer liquid crystals comprising bistolane mesogenic side groups," J. Appl. Phys. 106, 073505 (2009).
41. Ono, H., Emoto, A., Takahashi, F., Kawatsuki, N. and Hasegawa, T., "Highly stable polarization gratings in photocrosslinkable polymer liquid crystals," J. Appl. Phys. 94, 1298-1303 (2003).
42. Gao, K., McGinty, C., Payson, H., Berry, S., Vornehm, J., Finnemeyer, V., Roberts, B. and Bos, P., "High-efficiency large-angle Pancharatnam phase deflector based on dual-twist design," Opt. Express 25, 6283-6293 (2017).
43. Kakichashvili, S.D., "Method for phase polarization recording of holograms," Sov. J. Quantum Electron. 4, 795-798 (1974).
44. Crawford, G.P., Eakin, J.N., Radcliffe, M.D., Callan-Jones, A. and Pelcovits, R.A., "Liquid-crystal diffraction gratings using polarization holography alignment techniques," J. Appl. Phys. 98, 123102 (2005).
45. Chen, P., Wei, B.Y., Hu, W. and Lu, Y.Q., "Liquid-Crystal-Mediated Geometric Phase: From Transmissive to Broadband Reflective Planar Optics," Adv. Mater. 31, 1903665 (2019).
46. De Sio, L., Roberts, D.E., Liao, Z., Nersisyan, S., Uskova, O., Wickboldt, L., Tabiryan, N., Steeves, D.M., Kimball, B.R., "Digital polarization holography advancing geometrical phase optics," Opt. Express 24, 18297-18306 (2016).
47. Wu, H., Hu, W., Hu, H.C., Lin, X.W., Zhu, G., Choi, J.W., Chigrinov, V. and Lu, Y.Q., "Arbitrary photo-patterning in liquid crystal alignments using DMD based lithography system," Opt. Express 20, 16684-16689 (2012).
48. Yin, K., Xiong, J., He, Z. and Wu, S.T., "Patterning Liquid Crystal Alignment for Ultra-Thin Flat Optics," ACS Omega 5, 31485-31489 (2020).
49. Cakmakci, O. and Rolland, J., "Head-worn displays: a review," J. Display Tech. 2, 199-216 (2006).
50. Wang, J., Liang, Y. and Xu, M., "Design of a see-through head-mounted display with a freeform surface," JOSK 19, 614-618 (2015).
51. Saarikko, P., "Diffractive exit-pupil expander with a large field of view," Proc. SPIE 7001, 700105 (2008).
52. Äyräs, P., Saarikko, P. and Levola, T., "Exit pupil expander with a large field of view based on diffractive optics." J. Soc. Inf. Disp. 17, 659-664 (2009).
53. Xiang, X., Kim, J. and Escuti, M.J., "Bragg polarization gratings for wide angular bandwidth and high efficiency at steep deflection angles,"Sci. Rep. 8, 7202 (2018).
54. Broer, D.J., Lub, J., Mol, G.N., "Wide-band reflective polarizers from cholesteric polymer networks with a pitch gradient," Nature 378, 467-469 (1995).
55. Yin, K., Lin, H.Y. and Wu, S.T., "Chirped polarization volume grating with ultra-wide angular bandwidth and high efficiency for see-through near-eye displays," Opt. Express 27, 35895-35902 (2019).
56. Yin, K., He, Z. and Wu, S.T., "Reflective polarization volume lens with small f-number and large diffraction angle," Adv. Opt. Mater. 8, 2000170 (2020).
57. Hoffman, D.M., Girshick, A.R., Akeley, K., Banks, M.S., "Vergence-accommodation conflicts hinder visual performance and cause visual fatigue," J. Vis. 8, 33 (2008).

58. Hua, H., “Enabling focus cues in head-mounted displays,” Proc. IEEE 105, 805-824 (2017).
59. He, Z., Yin, K. and Wu, S.T., “Passive polymer-dispersed liquid crystal enabled multi-focal plane displays,” Opt. Express 28, 15294-15299 (2020).
60. Arimoto, H. and Javidi, B., “Integral 3D imaging with digital reconstruction,” Opt. Lett. 26, 157-159 (2001).
61. Huang, F.C., Chen, K. and Wetzstein, G., “The light field stereoscope: immersive computer graphics via factored near-eye light field displays with focus cues,” ACM Trans. Graph. 34, 1-12 (2015).
62. Wakunami, K., Hsieh, P.Y., Oi, R., Senoh, T., Sasaki, H., Ichihashi, Y., Okui, M., Huang, Y.P. and Yamamoto, K., “Projection-type see-through holographic three-dimensional display,” Nat. Commun. 7, 12954 (2016).
63. Li, G., Lee, D., Jeong, Y., Cho, J. and Lee, B., “Holographic display for see-through augmented reality using mirror-lens holographic optical element,” Opt. Lett. 41, 2486-2489 (2016).